Journal of Fluorine Chemistry 144 (2012) 157–164

Contents lists available at SciVerse ScienceDirect

Journal of Fluorine Chemistry

journal homepage: www.elsevier.com/locate/fluor

Controllable synthesis, upconversion luminescence, and paramagnetic properties of $NaGdF_4:Yb^{3+},Er^{3+}$ microrods

Zhe Chen, Zhenyu Liu, Ye Liu, Kezhi Zheng *, Weiping Qin *

State Key Laboratory on Integrated Optoelectronics, College of Electronic Science and Engineering, Jilin University, Changchun 130012, China

ARTICLE INFO

Article history:
Received 26 April 2012
Received in revised form 18 August 2012
Accepted 29 August 2012
Available online 4 September 2012

Keywords:
Morphologies
Growth mechanism
Upconversion emissions
Paramagnetic features

ABSTRACT

Hexagonal phase $NaGdF_4$ microrods have been successfully synthesized via a facile hydrothermal method with ethylene diamine tetraacetic acid (EDTA) as the structure-directing agent. The additive amounts of NaF and $NaNO_3$ as well as the reaction time have great effect on the morphology evolution of the products. A possible growth mechanism was proposed for the formation of β-$NaGdF_4$ microrods. Under the excitation of 980 nm near-infrared laser, bright green upconversion (UC) emissions can be readily achieved from $NaGdF_4$:10%Yb^{3+},1%Er^{3+} microrods. In addition, the $NaGdF_4$ microrods exhibit excellent paramagnetic features with the magnetization value of 5.02 emu/g (18 kOe) at room temperature. Both the UC luminescent and magnetic properties are closely related to the size of as-prepared products. These multifunctional β-$NaGdF_4$ microrods would have potential applications in the fields such as solid-state lasers, lighting, displays, and magnetic resonance imaging (MRI), and so on.

1. Introduction

In modern chemistry and materials science, rare earth (RE) fluorides with the formula of $(RE)F_3$ or $A(RE)F_4$ (A = alkaline metal, RE = rare earth elements) have aroused much attention because of the unique electronic and optical properties [1–6]. With doping trivalent lanthanide ions (Ln^{3+}), these compounds might possess prominent luminescent features [7] and magnetic properties based on the 4f electrons in lanthanide ions [8,9]. All these properties are highly depend on the size and shape of as-synthesized nano-/micro-scale particles. Therefore, to elucidate their shape- and size-dependent properties, most efforts have been made to the controllable synthesis of nano/microcrystals in recent years [10–17]. Among the RE fluoride hosts, sodium rare earth fluorides ($NaREF_4$) are regarded as the most outstanding host lattices for upconversion (UC) luminescence due to their low phonon energies [3–5,18–20]. As one typical example in them, $NaGdF_4$ possesses some unique physical properties which originate from Gd^{3+} ions. Firstly, since the lowest excited state $^6P_{7/2}$ of Gd^{3+} locates in the ultraviolet region, the energy transfers from other lanthanide ions such as Er^{3+}, Tm^{3+}, and Ho^{3+} to Gd^{3+} are effectively cut off in visible–infrared region, which decrease the excitation energy loss and improve the luminescence efficiency in UC processes [21]. Secondly, Gd^{3+} can serve as an intermediate ions to pass the excited energy from sensitizers (e.g. Yb^{3+}/Tm^{3+} ions pair) to activators ions (e.g. Tb^{3+}, Eu^{3+}, and Sm^{3+}), and consequently facilitate the energy transfer processes in fluoride phosphors [22]. Thirdly, Gd^{3+} ion is widely known as an ideal paramagnetic relaxation agent because of its large magnetic moment and nanosecond time scale electronic relaxation time [23]. Therefore, $NaGdF_4$ has been used in biological fields, such as bioseparation and paramagnetic relaxation agents in magnetic resonance imaging (MRI) [24].

Up to now, most of the reported researches, to our best knowledge, are predominantly focused on the controllable fabrication of Ln^{3+} doped $NaGdF_4$ nanocrystals (NCs) in both cubic and hexagonal phase owing to their promising applications in biolabel, bioseparation, and so on [12,19,24–29]. However, there are few reports on the manufacture of single-crystal $NaGdF_4$ with uniform size and well-defined shape at submicron or even micron scale, let alone the further studies of their UC luminescent and paramagnetic properties [30,31]. Furthermore, compared with NCs, $NaGdF_4$ microcrystals (MCs) might have many novel chemical, optical, magnetic, and electrical properties. Therefore, it is also significant for researchers to synthesize $NaGdF_4$ MCs with controllable shape and size and further investigate their optical and magnetic properties.

In this article, well-defined hexagonal phase $NaGdF_4$ microrods prepared via facile hydrothermal method are reported. The controllable regulation of crystalline phase, morphology, and size of as-synthesized products can be performed by adjusting the amounts of NaF and $NaNO_3$. More significantly, the unique formation process of β-$NaGdF_4$ MCs is revealed through a time-controlled experiment. The size-dependent properties of UC luminescence and paramagnetism are also investigated in detail.

* Corresponding authors. Tel.: +86 431 85168241; fax: +86 431 85168241.
E-mail address: wpqin@jlu.edu.c (W. Qin).

0022-1139/$ – see front matter © 2012 Elsevier B.V. All rights reserved.
http://dx.doi.org/10.1016/j.jfluchem.2012.08.009

These multifunctional microrods would have potential applications in solid-state laser, lighting, displays, MRI, etc.

2. Results and discussion

Generally, controllable synthesis of rare earth compounds in a solution-based system not only depends on the intrinsic structure of the target compounds but also requires precisely setting some growth parameters such as surfactants, the pH value of precursor solution, reaction temperature and time, and so on. In our designed system, we mainly focus on three effects on the final composition, morphology, and size of the as-synthesized products, including the molar ratio of NaF to Gd^{3+}, the addition amount of $NaNO_3$, and the reaction time, which will be discussed in the following paragraphs seriatim.

2.1. Effects of NaF and $NaNO_3$ additive amount on final products

To investigate the possible effects of varied NaF content on final products, the NaF/Gd^{3+} ratio was selectively regulated from 6 to 12 with other synthetic conditions unchanged. As can be seen from Fig. 1a, when the NaF/Gd^{3+} ratio is 6, the sharp diffraction peaks which indicate the high crystallization of products can be well assigned to orthorhombic phase GdF_3 (JCPDS card no.12-0788). The corresponding SEM image (Fig. 2a) reveals that the morphology is uniform lotus-like NCs which formed from an ordered assembly of numerous rice-like nanoparticles with the mean particle size of about 110 nm. When the ratio reaches 7, some new diffraction peaks appear; as shown in Fig. 1b, and they can be rightly indexed to the hexagonal phase $NaGdF_4$ (JCPDS card no. 27-0699). Fig. 2b illustrates that these emerging $NaGdF_4$ are hexagonal microrods. Their average diameter and length are ~0.7 μm and ~1.6 μm, respectively. However, a large number of brick-like nanoparticles emerge instead of the original lotus-like GdF_3 NCs. With the continuous increase of the ratio to 8, the diffraction peaks from β-$NaGdF_4$ increase and the diffraction peaks from GdF_3 decrease, as shown in Fig. 1c. It is clearly observed from Fig. 2c that the corresponding morphologies are well-shaped hexagonal microrods and minor rice-like nanoparticles. Based on the above description, it is worth noting that the morphology of as-obtained GdF_3 alters with increasing the additive content of NaF

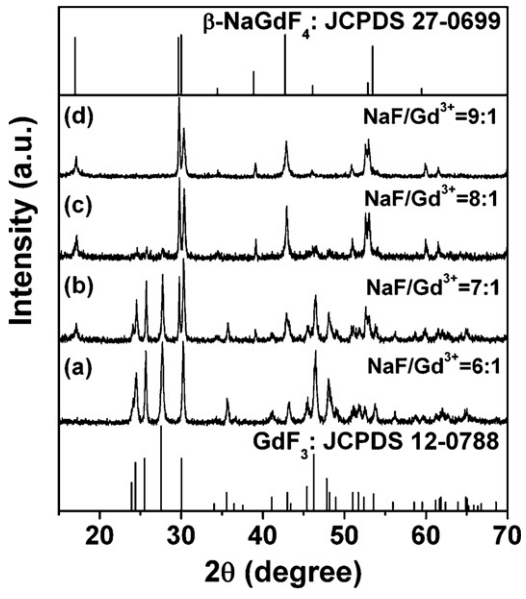

Fig. 1. XRD patterns of the products with different molar ration of NaF to Gd^{3+}. (a) NaF/Gd^{3+} = 6:1; (b) NaF/Gd^{3+} = 7:1; (c) NaF/Gd^{3+} = 8:1; (d) NaF/Gd^{3+} = 9:1.

regularly. More significantly, with the increase of NaF addition, the final products can transform from GdF_3 to $NaGdF_4$. When the NaF/Gd^{3+} ratio comes to 9, the final products can completely convert to pure hexagonal $NaGdF_4$ microrods, as can be seen from Figs. 1d and 2d. According to the above results, we can conclude that the composition, shape and crystalline phase of the as-synthesized products are seriously affected by the critical reacting amount of NaF with other synthetic parameters keeping unchanged.

To illustrate the variation of crystal structure of final products, the possible reaction processes for the formation of both GdF_3 and $NaGdF_4$ are summarized as follows:

$$Gd^{3+} + EDTA^{4-} \rightarrow Gd^{3+} - EDTA^{4-} \ (\text{complex}) \quad (1)$$

$$Gd^{3+} - EDTA^{4-} + Na^{+} + 4F^{-} \rightarrow NaGdF_4 + EDTA^{4-} \quad (2)$$

$$Gd^{3+} - EDTA^{4-} + 3F^{-} \rightarrow GdF_3 - EDTA^{4-} \quad (3)$$

Based on the comparison between Eqs. (2) and (3), it can be concluded that the lack of F^- ions will make the formation of $NaGdF_4$ much more difficult than that of GdF_3. Therefore, it is easier to obtain GdF_3 NCs rather than $NaGdF_4$ MCs at the low ratio of NaF/Gd^{3+}, as presented in Fig. 1a. When increasing NaF gradually, the concentration of F^- ions is enough and Eq. (2) is the primary reaction process instead of Eq. (3). Thus, $NaGdF_4$ MCs are obtained under high ratio of NaF/Gd^{3+}, which is in good agreement with the above experimental results. Lin et al. have reported that improving the pH value of mother liquor can make the composition transformation from GdF_3 to $NaGdF_4$ [32]. They proposed that the low pH value is favorable to the synthesis of GdF_3 and $NaGdF_4$ is preferred under high pH value. In our case, the original pH value of mother liquor is fixed at about 3, accompanied by the low reactants ratio of NaF/Gd^{3+}, which make GdF_3 NCs form inevitably. However, when the ratio of NaF to Gd^{3+} continues increasing to 9, 10, and even 12, the as-obtained samples become to pure hexagonal $NaGdF_4$ microrods, as shown in Fig. 2d–f. Especially, the corresponding TEM images and SAED pattern of the obtained $NaGdF_4$ microrods synthesized at the ratio of 10 are presented in Fig. 3, which can directly confirm the single crystal characteristic of the microrods. It can be clearly found that the diameter of as-synthesized $NaGdF_4$ microrods decrease whereas the slenderness ratio of these $NaGdF_4$ microrods increase with increasing the molar ratio of NaF to Gd^{3+}, which is well depicted in Fig. 4. The specific reason for this phenomenon will be given below.

In addition, further comparison between Eqs. (2) and (3) reveals that the addition of Na^+ might be another effective route to obtain $NaGdF_4$. Hence, parallel experiments are performed by adding $NaNO_3$ as additional mineralizer at the NaF/Gd^{3+} ratio of 6 with other condition parameters unchanged. XRD patterns and SEM images of the as-synthesized samples prepared by adding different amount of $NaNO_3$ are shown in Figs. 5 and 6, respectively. With increasing the addition of $NaNO_3$ from 2 to 50 mmol, the final products can transform from GdF_3 to $NaGdF_4$, which can be confirmed from Fig. 5. Furthermore, as clearly depicted in Fig. 6, the corresponding morphology experiences the transformation from originally lotus-like NCs to the mixture of lotus-like NCs and hexagonal microrods and finally to the pure hexagonal $NaGdF_4$ microrods. Therefore, improving the concentration of Na^+ is indeed a practical way to obtain β-$NaGdF_4$ MCs.

As discussed in above paragraphs, the reactants molar ratio of NaF to Gd^{3+} can greatly influence the size and the slenderness ratio of as-obtained β-$NaGdF_4$ microrods. In current synthetic system, with increasing the addition of NaF, F^- becomes excessive compared with Gd^{3+} and the redundant F^- will cap on the crystal surface inevitably due to the strong coordination effect between F^- and Gd^{3+}. According to Gibbs–Thompson theory, the relative

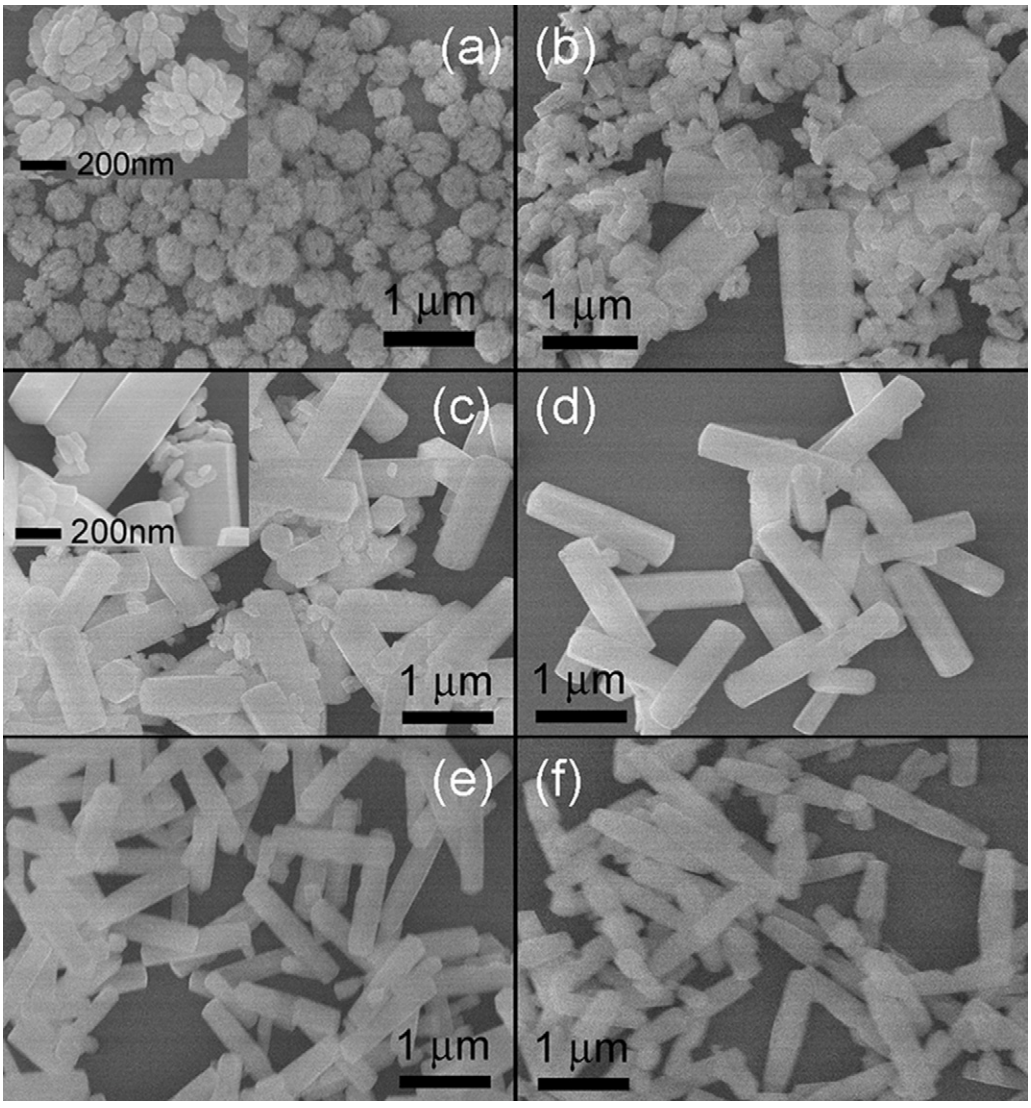

Fig. 2. Effect of the molar ratio of NaF to Gd^{3+} on the as-prepared products. (a) NaF/Gd^{3+} = 6:1, lotus-like NCs; (b) NaF/Gd^{3+} = 7:1, brick-like NCs and microrods; (c) NaF/Gd^{3+} = 8:1, rice-like NCs and microrods; (d–f) NaF/Gd^{3+} = 9:1, 10:1, 12:1, pure microrods.

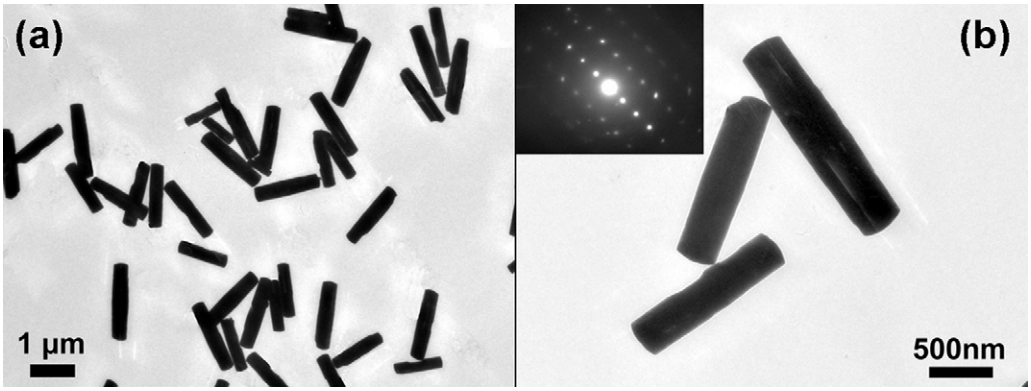

Fig. 3. TEM images and SAED pattern of $NaGdF_4$ microrods prepared at the NaF/Gd^{3+} = 10:1.

chemical potential of a crystal is simply proportional to its surface-atom ratio, which is determined by the average number of dangling bonds per atom over the entire crystal [33]. The capping effect of F^- would decrease the average number of dangling bonds, and further decrease the chemical potential of the crystal as well as that of crystal surface. Due to the density of Gd^{3+} on the $[1\,0\,\bar{1}\,0]$ crystal plane is higher than that on the [0 0 0 1] crystal plane, the selective absorption of F^- on the $[1\,0\,\bar{1}\,0]$ crystal plane would be greater than that on the [0 0 0 1] plane, and the similar interpretation has been illustrated clearly in β-$NaYF_4$ system

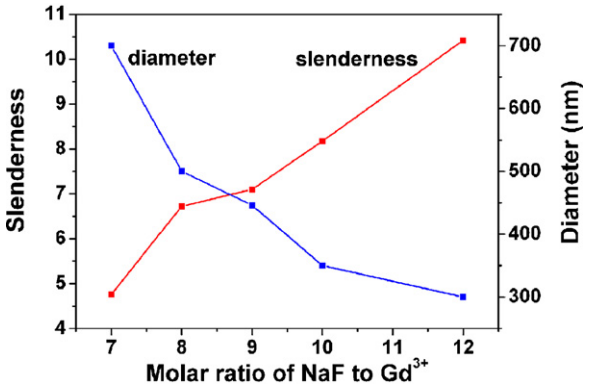

Fig. 4. The function image of the effect of the NaF/Gd^{3+} ratio on the size of obtained $NaGdF_4$ microrods.

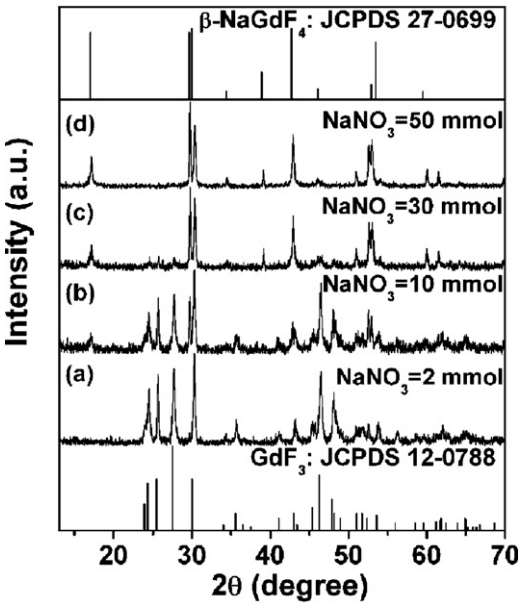

Fig. 5. XRD patterns of the obtained products with different addition of $NaNO_3$. (a) 2 mmol; (b) 10 mmol; (c) 30 mmol; (d) 50 mmol.

[34]. Then, as described above, the surface energy of the $[1\,0\,\bar{1}\,0]$ crystal plane will be certain to decrease dramatically while that of the [0 0 0 1] crystal plane increases relatively. As a result, the relative growth rate along [0 0 0 1] is much quicker than that along $[1\,0\,\bar{1}\,0]$, finally leading to larger aspect ratio of microrods at higher NaF/Gd^{3+} ratio, as shown in Fig. 4.

Additionally, the effects of the amount of EDTA on the morphologies of final products are also discussed with other reaction conditions similar to **S5**. When decreasing the molar ratio of EDTA/Gd^{3+} from 1:1 to 0:1, the as-prepared β-$NaGdF_4$ microcrystals exhibit quite irregular shapes as shown in Fig. 7a. In addition, it can be clearly found in Fig. 7b that the top/bottom of the microrods becomes thinner than the middle parts when increasing the molar ratio of EDTA/Gd^{3+} to 2:1. The obvious changes in the final morphologies of as-prepared products can be mainly attributed to the selective adsorption of $EDTA^{4-}$ on the different facets of growing $NaGdF_4$ crystallites, giving rise to the difference of the growth rates between different crystallographic directions and forming the various morphologies and sizes [35]. In addition, the effects of excessive EDTA on final products (Fig. 7b) further confirm the existence of selective binding. To sum up, it is clear that EDTA plays critical roles as a structure-directing reagent binding to the surface of crystals selectively, resulting in different well-defined morphologies.

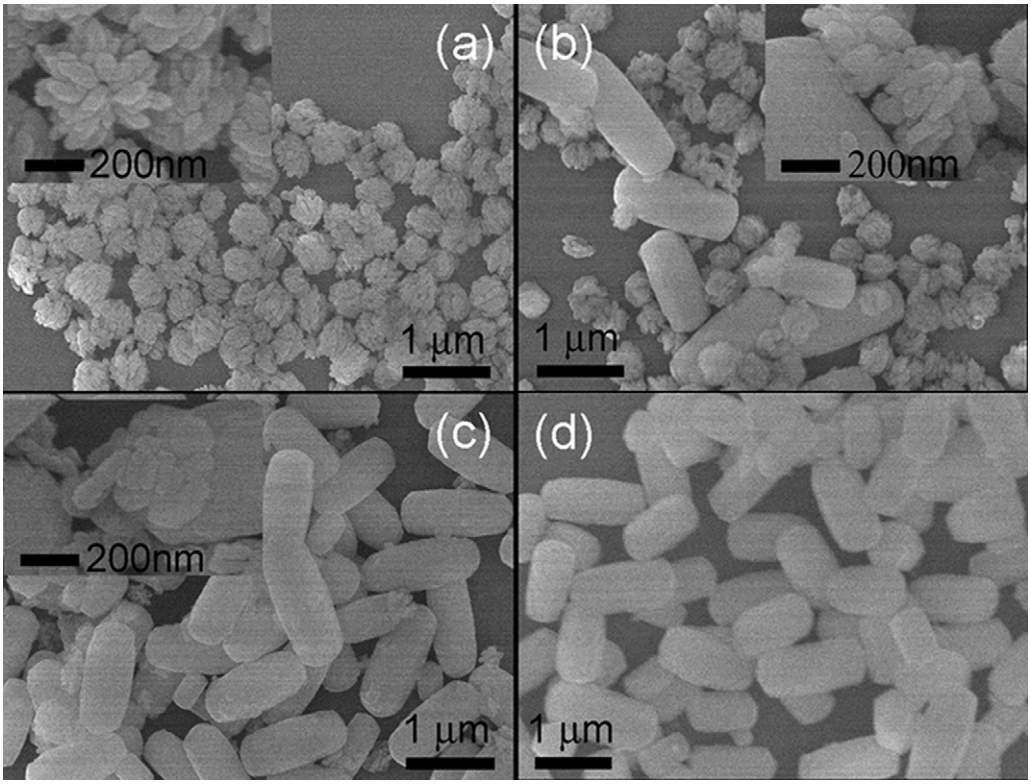

Fig. 6. The effects of the addition amount of $NaNO_3$ on the composition of final products of **S2**. (a) 2 mmol, lotus-like NCs; (b) 10 mmol, lotus-like NCs and microrods; (c) 30 mmol, rice-like NCs and microrods; (d) 50 mmol, pure microrods.

Fig. 7. TEM images of β-$NaGdF_4$ microcrystals synthesized with different amount of EDTA and other conditions are similar to **S5**. (a) Irregular microcrystals at EDTA/Gd^{3+} = 0:1; (b) spindle-like microcrystals at EDTA/Gd^{3+} = 2:1.

2.2. Formation mechanism of β-$NaGdF_4$ microrods

The formation procedure of as-synthesized crystals undergoes a two-step growth process as follows: (1) the formation of crystal nuclei, and (2) further crystal growth from the nuclei along with the reaction time. Here, **S5** is chosen to perform time-controlled experiments for the detailed investigation of inherent crystal growth mechanism. In the nucleation stage, the possible reaction processes for the formation of $NaGdF_4$ crystal nuclei have been shown in Eqs. (1) and (2), as described above. As $NaGdF_4$ crystal nuclei formed in the mother liquor, further crystal growth would carry out immediately. As shown in Fig. 9a, the as-obtained products under hydrothermal treatment for only 15 min are composed of spindle-like MCs with average length of 1.1 μm and spherical nanoparticles with about 0.28 μm in diameter. The various morphologies of products are in accordance with the co-existence of diffraction peaks of cubic and hexagonal phase $NaGdF_4$ as shown in the corresponding XRD pattern. The extremely weak diffraction peaks, as depicted in Fig. 8a, demonstrate that high crystallinity cannot be achieved in such short reaction time. When the reaction time increases to 30 min, the well-formed spindle-like $NaGdF_4$ MCs, as well as the spherical $NaGdF_4$ nanoparticles, become big and smooth, which are presented well in Fig. 9b. Accordingly, the diffraction peaks of both cubic and hexagonal phase $NaGdF_4$ become intense and sharp as shown in Fig. 8b. When the reaction time continues elongating to 1 h, a large number of well-defined hexagonal microrods appeared with other spherical nanoparticles became smaller than before (Fig. 9c), which results in the higher intensity of hexagonal phase peaks than those of cubic phase, as shown in Fig. 8c. The above results indicate that the transformation from cubic to hexagonal phase is proceeding with prolonging the reaction time. Finally, when extending the reaction time to 2 h, the cubic phase $NaGdF_4$ completely converted to hexagonal phase and all the obtained products are of pure hexagonal microrods with average length of about 1.55 μm, as shown in Figs. 8d and 9d, respectively. From free energy viewpoint, the crystal growth is processed towards more stable direction in thermodynamics. It is well known that hexagonal phase is a more thermodynamically stable phase than cubic phase [36]. In the synthesis process, owing to the reaction is carried out under high temperature and high pressure conditions, the sufficient supply of thermal energy makes the final products become stable hexagonal phase rather than the initial cubic phase. In other words, a dissolution–recrystallization (D–R) process, which means the dissolution of metastable α phase particles to serve as the component source for the further growth of β phase, inevitably occurs in the phase transformation process. It is worth to note that the simultaneous formation of cubic and hexagonal phase $NaGdF_4$ at the early stage in reaction process (Fig. 8a) is different from pure cubic phase obtained in the synthesis of $NaYF_4$ [37]. This difference could be attributed to the difference in ionic radii between Gd^{3+} and Y^{3+}. Theoretically, the light lanthanides with large ionic radii exhibit a high tendency towards electron cloud distortion owing to the increased dipole polarizability, and thus favor the hexagonal structure [21]. Therefore, $NaGdF_4$, doped with bigger Gd^{3+} ions than Y^{3+}, will prefer to form hexagonal phase than $NaYF_4$.

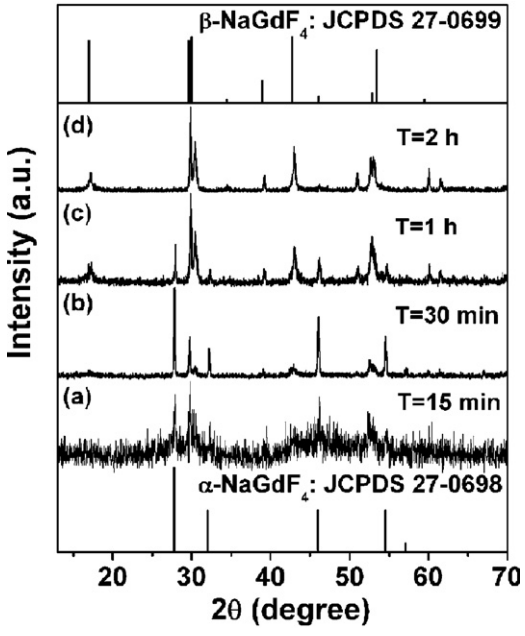

Fig. 8. XRD patterns of samples at different reaction time of (a) 15 min; (b) 30 min; (c) 1 h; (d) 2 h.

Based on the above analysis, it can be concluded that, besides inherent unit cell structures of nucleated seeds, reaction time is also a key factor in the phase and morphology evolution of the final products. Scheme 1 summarizes the possible formation processes of β-$NaGdF_4$ microrods under various experimental conditions.

2.3. Upconversion luminescent properties

The UC luminescence of Ln^{3+} has been investigated extensively because of their potential applications in various fields, such as lighting, display, IR detection, and medical imaging [38,39]. Here, to verify the UC luminescence properties in our materials, **S4**, **S5** and **S6** are selected as hosts to prepare β-$NaGdF_4$: 10%Yb^{3+}/1%Er^{3+}

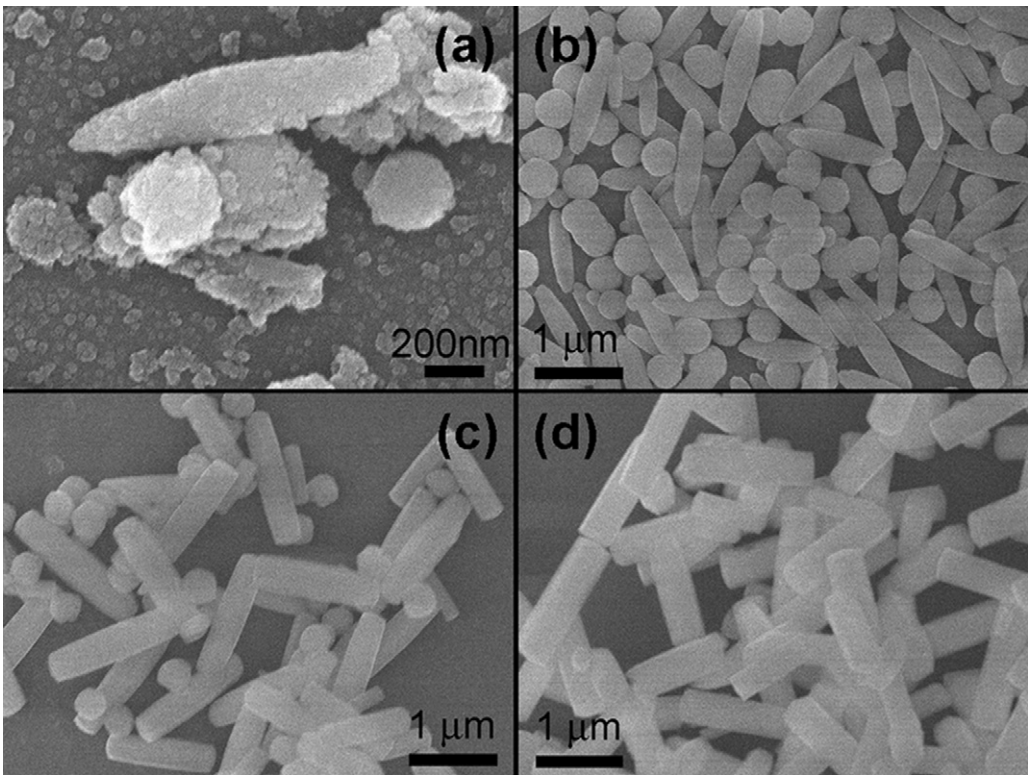

Fig. 9. SEM images of samples at different reaction time of (a) 15 min; (b) 30 min; (c) 1 h; (d) 2 h.

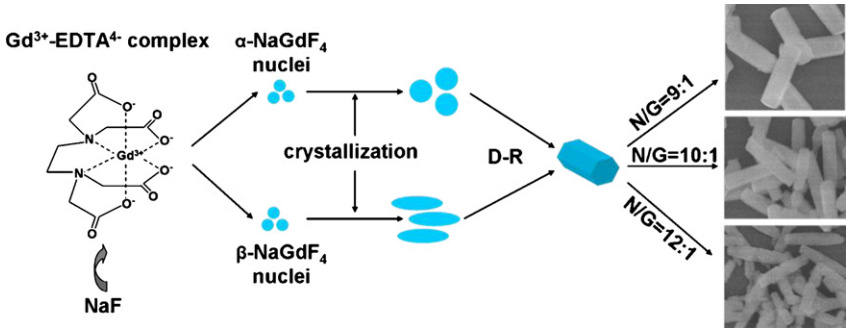

Scheme 1. Schematic illustration for the formation process of $NaGdF_4$ microrods (D–R and N/G represent dissolution–recrystallization and the molar ratio of NaF to Gd^{3+}, respectively).

MCs which are labeled as **S4#**, **S5#** and **S6#**, respectively. Fig. 10a shows the UC luminescence spectra of **S4#**, **S5#** and **S6#** under the excitation of 980 nm near-infrared laser with a pump-power density of ~140 mW/cm^2. All samples exhibit typical emission bands of Er^{3+} in visible region, including purple emission (centered at 408 nm), green emission bands (centered at 520 and 545 nm) and red emission (centered at 664 nm). According to the simplified energy diagram shown in Fig. 10b, the above UC emissions can be well assigned to $^2H_{9/2} \rightarrow {}^4I_{15/2}$, $^2H_{11/2}/{}^4S_{3/2} \rightarrow {}^4I_{15/2}$ and $^4F_{9/2} \rightarrow {}^4I_{15/2}$ transitions of Er^{3+}, respectively [40,41]. The possible UC population processes are given in Fig. 10b as well. In addition, it is worth noting that the whole UC emission intensity of samples decreases with increasing the molar ratio of NaF to Gd^{3+}, as shown in Fig. 10a, which is mainly attributed to the surface quenching effect [42]. It is well known that each emission peak include a sum of optical emissions contributed from doped ions both at the surface and in the interior of the particles. Compared with the interior doped ions, the surface doped ions should show weakened emissions owing to the quench of excitation energy by surface defects [43]. From the inset of Fig. 10a, we found that the specific surface area of β-$NaGdF_4$ microrods increases with the increase of molar ratio of NaF to Gd^{3+}. The larger specific surface area is, the more surface quenching centers are. In addition, as shown in Fig. 2f, **S6#** shows obvious coarse surface which may also contribute to the surface quenching effect. Thus, **S6#** exhibits great weaker UC luminescence than **S5#** and **S4#**.

2.4. Paramagnetic properties of $NaGdF_4$ microrods

Apart from the UC luminescence property, the magnetism of $NaGdF_4$ microrods is also investigated. Fig. 11 shows the room-temperature magnetization (M) values of $NaGdF_4$ microrods originating from **S4#**, **S5#**, and **S6#**, respectively, as a function of applied field (H) (−18–18 kOe). It is clear that all samples exhibit obvious paramagnetism. The paramagnetic property of the Gd^{3+} ions in $NaGdF_4$ microrods comes from seven unpaired inner 4f electrons which are closely bound to the nucleus and effectively shielded by the outer closed-shell electrons $5s^25p^6$ from the crystal

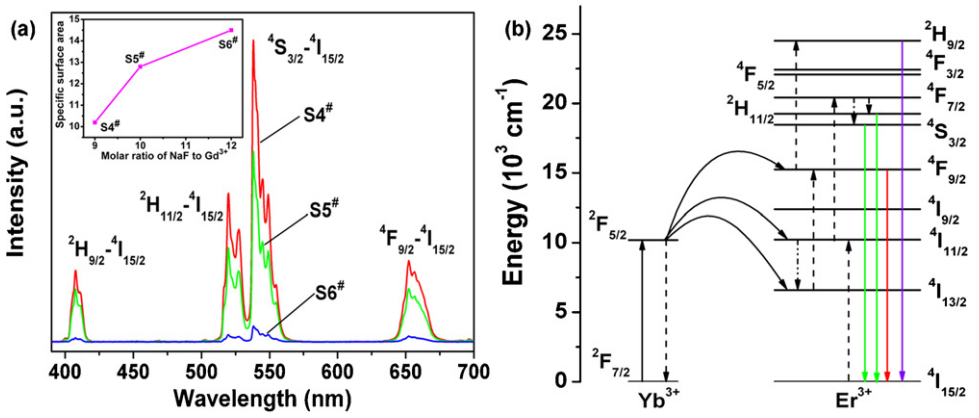

Fig. 10. The UC luminescence properties of $NaGdF_4$:10%Yb^{3+}/1%Er^{3+} microrods. (a) UC luminescence spectra of samples derived from **S4**#, **S5**# and **S6**#, respectively. (b) Schematic energy level diagram of Yb^{3+} and Er^{3+}, and proposed mechanism of UC emissions. Inset of (a) is the function image of the effect of NaF/Gd^{3+} ratio on the specific surface area of **S4**#, **S5**# and **S6**#.

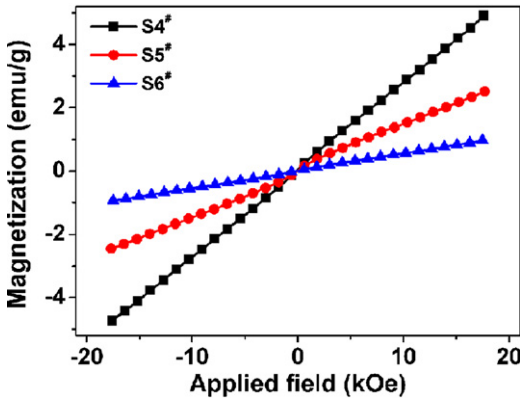

Fig. 11. Magnetization as a function of applied field for $NaGdF_4$ microrods originated from **S4**#, **S5**#, and **S6**#, separately.

field. The magnetic moment associated with the Gd^{3+} ions are all localized and noninteracting, giving rise to paramagnetism [44]. The mass magnetic susceptibility values of **S4**#, **S5**#, and **S6**# are determined to be 27.9×10^{-5}, 13.9×10^{-5}, and 5.3×10^{-5} emu/g Oe, respectively. The magnetization values of **S4**#, **S5**#, and **S6**# at 18 kOe are about 5.02, 2.50, and 0.95 emu/g, which are near to the reported value of the nanoparticles used for common bioseparation [45]. In addition, by comparing the magnetization of these three samples, it can be inferred that the magnetization of $NaGdF_4$ microrods seriously depends on their size. This size-dependent property may be closely related with the different distribution of Gd^{3+} in host materials, which need further theory and experimental studies.

3. Conclusion

In summary, controllable synthesis of gadolinium fluorides with different compositions (GdF_3 and $NaGdF_4$) and various morphologies (lotus-like particles, rice-like NCs, and microrods) is achieved by preciously adjusting the addition of NaF and $NaNO_3$ through hydrothermal method. The time-dependent experiment confirms the phase transition from α-$NaGdF_4$ to β-$NaGdF_4$ with prolonging the reaction time. By doping the Yb^{3+}–Er^{3+} ion pair, these β-$NaGdF_4$ microrods present excellent size-dependent UC luminescence property. The size dependence of paramagnetic properties is also obtained in these β-$NaGdF_4$ microrods. Hopefully, the luminescent and paramagnetic properties can make these microrods be promising multifunctional materials and have potential applications in solid-state lasers, lighting, FEDs, MRI and so on.

4. Experimental

4.1. Samples preparation

The rare earth nitrates $RE(NO_3)_3 \cdot 6H_2O$ (RE = Gd, Yb, Er) were purchased from Shanghai Shabo Chemical Reagent Company and other chemicals were purchased from Beijing Chemical Company, China. All the chemicals were of analytical grade and used without further purification.

In a typical synthesis of $NaGdF_4$, 1 mL $Gd(NO_3)_3$ (0.5 M) solution was poured into an 10 mL of aqueous solution containing 0.5 mmol of EDTA. After vigorously stirring for 30 min, 5 mmol NaF was added into the above solution. After another additional agitation for 30 min, the obtained mixing solution was transferred into a 30 mL Teflon-lined stainless steel autoclave, and then heated to 180 °C for 24 h. After the autoclave was cooled to room temperature naturally, the resulting precipitates were isolated by centrifugation, washed with deionized water and ethanol in sequence, and dried in air. All the synthetic conditions and characteristics of samples prepared via hydrothermal route were listed in Table 1. The as-synthesized products were labeled from **S1** to **S6** according to the different addition amount of NaF. Furthermore, sodium nitrate ($NaNO_3$) can be used as the additional mineralizer in the experiments, and the corresponding products were labeled from **S7** to **S10** on the basis of different $NaNO_3$ addition. To investigate the luminescence properties of Ln^{3+} ions in Ln^{3+} doped $NaGdF_4$ microcrystals, the Yb^{3+}–Er^{3+} codoped $NaGdF_4$

Table 1
Parameters of the representative experiments and the morphologies of the corresponding products.

Sample	NaF/Gd^{3+}	$NaNO_3$ (mmol)	pH	Product	Morphology
S1	6:1	0	3	GdF_3	Lotus
S2	7:1	0	3	β-$NaGdF_4$ and GdF_3	Rod and brick
S3	8:1	0	3	β-$NaGdF_4$ and GdF_3	Rod and rice
S4	9:1	0	3	β-$NaGdF_4$	Rod
S5	10:1	0	3	β-$NaGdF_4$	Rod
S6	12:1	0	3	β-$NaGdF_4$	Rod
S7	6:1	2	3	GdF_3	Lotus
S8	6:1	10	3	GdF_3 and β-$NaGdF_3$	Lotus and rod
S9	6:1	30	3	β-$NaGdF_4$ and GdF_3	Rod and rice
S10	6:1	50	3	β-$NaGdF_4$	Rod

samples were prepared by introducing certain amount of $Yb(NO_3)_3$ and $Er(NO_3)_3$ solution into the solution as described above.

4.2. Characterization

The crystal structure was analyzed by a Rigaku RU-200b X-ray powder diffractometer (XRD) using a nickel-filtered Cu-Kα radiation (λ = 0.15406 nm). The size and morphology were investigated by a JEOL JSM-6330F field emission scanning electron microscope (FESEM). The UC photoluminescence emission spectra were recorded using a Hitachi F-4500 fluorescence spectrophotometer (1.0 nm for slit width and 400 V for photo multiplier tube voltage) with a 980 nm continuous wave diode laser as the excitation source. Magnetic properties were measured using a vibrating sample magnetometer. All the measurements were performed at room temperature.

Acknowledgments

This work was supported by the National High Technology Research and Development Program of China (863 Program: 2009AA03Z309), the National Natural Science Foundation of China (NSFC) (grants 51072065, 60908031 and 60908001) and the Program for New Century Excellent Talents in University (No: NCET-08-0243).

References

[1] P.A. Tanner, J.W. Wang, Journal of the American Chemical Society 132 (2010) 947–949.
[2] P.A. Tanner, L.S. Fu, B.M. Cheng, Journal of Physical Chemistry C 113 (2009) 10773–10779.
[3] D.L. Shi, J. Lian, W. Wang, G.K. Liu, P. He, Z.Y. Dong, L.M. Wang, R.C. Ewing, Advanced Materials 18 (2006) 189–193.
[4] J. Larionova, E. Chelebaeva, Y. Guari, R.A.S. Ferreira, L.D. Carlos, F.A.A. Paz, A. Trifonov, C. Guerin, Inorganic Chemistry 48 (2009) 5983–5995.
[5] J. Rocha, M.H. Kostova, D. Ananias, F.A.A. Paz, A. Ferreira, L.D. Carlos, Journal of Physical Chemistry B 111 (2007) 3576–3582.
[6] L.D. Carlos, R.A.S. Ferreira, R.N. Pereira, M. Assuncao, V.D. Bermudez, Journal of Physical Chemistry B 108 (2004) 14924–14932.
[7] L.D. Carlos, R.A.S. Ferreira, V.D. Bermudez, S.J.L. Ribeiro, Advanced Materials 21 (2009) 509–534.
[8] F. Evanics, P.R. Diamente, F.C.J.M. van Veggel, G.J. Stanisz, R.S. Prosser, Chemistry of Materials 18 (2006) 2499–2505.
[9] R. Kumar, M. Nyk, T.Y. Ohulchanskyy, C.A. Flask, P.N. Prasad, Advanced Functional Materials 19 (2009) 853–859.
[10] F.C.J.M. van Veggel, R. Sivakumar, M. Raudsepp, Journal of the American Chemical Society 127 (2005) 12464–12465.
[11] S.V.S. Sivakumar, F.C.J.M. van Veggel, M. Raudsepp, Chemistry of Materials 17 (2005) 4736–4742.
[12] X.P. Fan, F. Wang, M.Q. Wang, Y. Zhang, Nanotechnology 18 (2007) 25701.
[13] G.S. Yi, H.C. Lu, S.Y. Zhao, G. Yue, W.J. Yang, D.P. Chen, L.H. Guo, Nano Letters 4 (2004) 2191–2196.
[14] X.G. Liu, F. Wang, Chemical Society Reviews 38 (2009) 976–989.
[15] J.A. Capobianco, J.C. Boyer, L.A. Cuccia, Nano Letters 7 (2007) 847–852.
[16] M. Haase, S. Heer, K. Kompe, H.U. Gudel, Advanced Materials 16 (2004) 2102–2105.
[17] Y. Zhang, Z.Q. Li, S. Jiang, Advanced Materials 20 (2008) 4765–4769.
[18] P.R. Diamente, M. Raudsepp, F.C.J.M. van Veggel, Advanced Functional Materials 17 (2007) 363–368.
[19] M. Haase, P. Ptacek, H. Schafer, K. Kompe, Advanced Functional Materials 17 (2007) 3843–3848.
[20] Y.W. Zhang, H.X. Mai, R. Si, Z.G. Yan, L.D. Sun, L.P. You, C.H. Yan, Journal of the American Chemical Society 128 (2006) 6426–6436.
[21] X.G. Liu, F. Wang, Y. Han, C.S. Lim, Y.H. Lu, J. Wang, J. Xu, H.Y. Chen, C. Zhang, M.H. Hong, Nature 463 (2010) 1061–1065.
[22] F. Wang, R.R. Deng, J. Wang, Q.X. Wang, Y. Han, H.M. Zhu, X.Y. Chen, X.G. Liu, Nature Materials 10 (2011) 968–973.
[23] F.C.J.M. van Veggel, F. Evanics, P.R. Diamente, G.J. Stanisz, R.S. Prosser, Chemistry of Materials 18 (2006) 2499–2505.
[24] N.J.J. Johnson, W. Oakden, G.J. Stanisz, R. Scott Prosser, F.C.J.M. van Veggel, Chemistry of Materials 23 (2011) 3714–3722.
[25] D.P. Chen, C.H. Liu, H. Wang, X.R. Zhang, Journal of Materials Chemistry 19 (2009) 489–496.
[26] B. Yan, Q. Zhang, Chemical Communications 47 (2011) 5867–5869.
[27] J.A. Capobianco, J.C. Boyer, J. Gagnon, L.A. Cuccia, Chemistry of Materials 19 (2007) 3358–3360.
[28] J.A. Capobianco, R. Naccache, F. Vetrone, V. Mahalingam, L.A. Cuccia, Chemistry of Materials 21 (2009) 717–723.
[29] R. Song, J. Ryu, H.Y. Park, K. Kim, H. Kim, J.H. Yoo, M. Kang, K. Im, R. Grailhe, Journal of Physical Chemistry C 114 (2010) 21077–21082.
[30] F. He, P.P. Yang, D. Wang, N. Niu, S.L. Gai, X.B. Li, Inorganic Chemistry 50 (2011) 4116–4124.
[31] J.H. Hao, Z.L. Wang, H.L.W. Chan, Journal of Materials Chemistry 20 (2010)3178–3185.
[32] Y.A. Wu, C.X. Li, D.M. Yang, J. Lin, Journal of Colloid and Interface Science 354 (2011) 429–436.
[33] R.X. Yan, X.M. Sun, X. Wang, Q. Peng, Y.D. Li, Chemistry: A European Journal 11 (2005) 2183–2195.
[34] X. Liang, X. Wang, J. Zhuang, Q. Peng, Y.D. Li, Advanced Functional Materials 17 (2007) 2757–2765.
[35] C. Li, Z. Quan, P. Yang, S. Huang, H. Lian, J. Lin, Journal of Physical Chemistry C 112 (2008) 13395–13404.
[36] J.W. Zhao, Y.J. Sun, X.G. Kong, L.J. Tian, Y. Wang, L.P. Tu, J.L. Zhao, H. Zhang, Journal of Physical Chemistry B 112 (2008) 15666–15672.
[37] C.X. Li, J. Yang, Z.W. Quan, P.P. Yang, D.Y. Kong, J. Lin, Chemistry of Materials 19 (2007) 4933–4942.
[38] H. Schafer, P. Ptacek, K. Kompe, M. Haase, Chemistry of Materials 19 (2007) 1396–1400.
[39] L. Wang, Y. Li, Chemical Communications (2006) 2557–2559. http://pubs.rsc.org/en/Content/ArticleLanding/2006/CC/b604871d.
[40] K.Z. Zheng, D. Zhao, D.S. Zhang, N. Liu, W.P. Qin, Optics Letters 35 (2010) 2442–2444.
[41] S. Schietinger, L.D. Menezes, B. Lauritzen, O. Benson, Nano Letters 9 (2009) 2477–2481.
[42] F. Wang, J.A. Wang, X.G. Liu, Angewandte Chemie International Edition 49 (2010) 7456–7460.
[43] J.C. Boyer, M.P. Manseau, J.I. Murray, F.C.J.M. van Veggel, Langmuir 26 (2009) 1157–1164.
[44] H.T. Wong, H.L.W. Chan, J.H. Hao, Applied Physics Letters 95 (2009) 22512.
[45] H.H. Yang, S.Q. Zhang, X.L. Chen, Z.X. Zhuang, J.G. Xu, X.R. Wang, Analytical Chemistry 76 (2004) 1316–1321.